The data was generally consistent among all of the bolts, with the yield strength ranging from ~115 ksi to 122 ksi and the ultimate strength ranging from the ~160 ksi to 167 ksi. The average elongation was ~30% and the average reduction in area was ~42%. These values were consistent with published mechanical properties for Alloy X-750 material.

13.0 ANALYSIS OF HEAD-TO-SHANK TRANSITION

Additional examinations were performed to further characterize the head-to-shank transition in the bolts to determine if anomalies existed that may have contributed to the cracking. These examinations included: estimating the surface finish, determining the radius of curvature between the head and shank, measuring the angle between the underside of the head and the shank, and performing higher magnification metallographic examinations of the radius between the head and shank. All examinations were performed on bolt 240°-7 and bolt 300°-1 (mounted specimens and loose pieces, as appropriate) unless otherwise noted.

The surface finish was estimated to be 32 RMS or better for both bolts based on a low magnification visual examination. It should be noted that the surface finish was difficult to determine accurately due to oxide buildup and relatively small amount of available material, especially for bolt 240°-7.

An optical comparator was used to determine the radius of curvature on three bolts: the two noted above plus bolt 180°-3 selected at random. None of the radii were perfectly formed or smooth; however, they did not contain unusually sharp transitions or features that would have played a significant role in the crack initiation. Consequently, the radii were estimated based on the best curvature fit. The results were as follows: bolt 240°-7 was ~0.065"; bolt 300°-1 was ~0.069"; and bolt 180°-3 was ~0.080". Higher magnification stereo microscope photographs taken of the mounted cross sections are provided in Figure 121 through Figure 124. Each of these figures includes a semi-transparent circle that represents the best curvature fit.

Efforts were made to measure the angle between the underside of the head and the shank. It was determined that none of the bolts were conducive to this measurement due to the cracking; therefore, no valid data was obtained.

Higher magnification metallographic examinations were performed on the radius between the head and shank of the two mounted specimens. A three-frame montage was taken of each radius as shown in Figure 125 through Figure 128. The radii were not perfectly formed or smooth as noted earlier. In addition, there were a few wavy areas observed, e.g. toward the shank side of bolt 300°-1, but there did not appear to be any sharp transitions, machining grooves, or notches associated with the cracking. There was also no obvious evidence of surface cold work at any initiation region as previously noted in Section 8.0.

14.0 DISCUSSION

The visual examinations performed on the twelve (12) open cracks indicated a general crack pattern consisting of crack initiation at two diametrically opposing sides of the bolt in the head-to-shank transition region. The cracking extended upward into the bolt head at a ~35° angle relative to horizontal. Final fracture occurred when the two opposing cracks linked together near the center of the bolt. An analysis of the axis of symmetry (i.e. the line drawn between the two opposing initiations) indicated no clear pattern in the direction of the prevailing stresses, either within bolts removed from a particular clevis or between different clevises. This finding indicated the stresses were variable from bolt to bolt. It also could suggest that stresses redistribute and/or change direction as multiple bolts failed at a particular clevis location.

All of the thirteen (13) intact bolts contained cracking in the head/shank transition. No cracking was identified in the threaded region of any bolt. The amount of angled cracking varied among the bolts, from many angled cracks (e.g. 240°-7) to very minor angled cracking (e.g. 300°-1).

Four bolts were selected for destructive examinations. The bolts were chosen to capture several variables, including intact and broken bolts, bolts with highly angled cracks and bolts with minor angled cracks. The selected bolts originated from three separate clevis locations, 120°, 240°, and 300°. Two bolts were chosen from the 120° clevis, since this location experienced the greatest number of bolt failures (all 8 failed at this location).

High magnification SEM examinations performed on the open cracks indicated the fracture surface was essentially 100% intergranular fracture. One small area near the center of bolt 120°-2 was mixed mode fracture consisting of transgranular cleavage and ductile microvoid coalescence. Cross section metallographic examinations confirmed the branched intergranular nature of the cracking in all four bolts examined.

SEM/EDS analysis of a polished cross section prepared through the 300°-1 bolt identified titanium nitride precipitates (typically ~15 μm in size) and niobium titanium intermetallic compounds (typically ~20 μm in size). Carbon was not positively detected in any location, presumably because the carbides were very fine, i.e. <1 μm in size. Subsequent optical metallography using the dual etch technique confirmed the carbide size was <1 μm, which is smaller than the EDS excitation volume. Consequently, no conclusions could be drawn regarding the carbide type(s), i.e. $M_{23}C_6$ or MC, present in the material microstructure.

The optical metallographic examinations also revealed the discrete, banded nature of the microstructure. The banded regions contained both carbides and second phase precipitates such as titanium nitrides. The carbides were generally intragranular within the banded regions. Carbide coverage at the grain boundaries was estimated to be 25% or less. The microstructure contained a duplex grain structure consisting primarily of fine grains (ASTM 7-8), with some very large grains (ASTM 1-2). There was no evidence of surface cold work or other surface anomaly noted at any of the initiation regions.

The lack of cold work was confirmed during the Vickers microhardness testing, which indicated uniform microhardness values at the initiation regions, mid-crack, and in the bulk material away from the cracking. The average microhardness was ~400 HV at all locations. These results match the bulk Rockwell C hardness values, which averaged ~40 HRC and were consistent with those expected for Alloy X-750 material.

Mechanical testing was performed on several miniature tensile specimens machined from the threaded region of the bolts. The data was generally uniform for all of the bolts, with the yield strength ranging from ~115 ksi to ~122 ksi and the ultimate tensile strength ranging from ~160 ksi to ~167 ksi. The average elongation was ~30% and the average reduction in area was ~40%; all of these results are as expected for Alloy X-750 material.

Low magnification SEM examination of the tensile fracture surfaces indicated the fracture mode was mixed and consisted of intergranular (IG) facets and ductile microvoid coalescence. The presence of IG facets typically suggests that the material was embrittled by some mechanism. Ref. 1 provides a possible explanation: "Two-step age-hardening treatments after solution annealing tend to precipitate MC rather than $M_{23}C_6$ carbides. The MC-type carbides are principally titanium carbides, TiC, which are likely trapping sites for hydrogen and increase the stay time of hydrogen at the grain boundaries, thus increasing the likelihood of SCC. The presence of residual hydrogen in the bulk material could also be responsible for the IG fracture on the tensile specimens. However, since the mechanical properties (especially elongation and reduction in area values) were as expected for Alloy X-750 material, it is believed that the presence of IG facets on the fracture surface is not significant.

Chemical analysis results by ICP-MS were within the expected ranges for Alloy X-750 material. The results for niobium + tantalum and titanium were slightly below the specified values in one or two cases, but were considered to be within the uncertainty of the ICP-MS technique, especially when accounting for additional product tolerances permitted by the material specification (Ref. 3).

The laboratory results, including tensile testing, hardness and microhardness testing, metallographic and SEM examinations, and chemical analysis were all consistent with Alloy X-750 material heat treated in accordance with the reported two-step aging heat treatment. The literature indicates that Alloy X-750 in this heat treatment will have poor IGSCC resistance in a PWR environment (Ref. 1, 6, 7).

For SCC to occur, three conditions must be present: 1) a susceptible material, 2) tensile stresses, and 3) an environment capable of causing stress corrosion cracking in that material. Each of these conditions is discussed briefly below:

Material

The bolt microstructure consisted of a duplex grain structure and also contained discrete bands of carbides and other precipitates. The duplex structure and banding are both influenced by prior work in the material and indicate a lower solution annealing temperature was used (1,625°F or 885C), i.e. it was not sufficiently high enough to dissolve the carbides and precipitates. For maximum SCC resistance, a 2,000°F (1,093C) solution annealing temperature is recommended, followed by a single-step aging treatment. At the higher solution annealing temperature, all of the carbides are dissolved and can re-precipitate as $M_{23}C_6$ type carbides at the grain boundaries during subsequent aging. An added benefit of the higher temperature solution anneal is grain growth, which reduces the grain boundary volume, thereby increasing resistance to IGSCC.

Tensile Stress

The prevailing stresses on the bolts were applied tensile stresses. An analysis of the fracture surfaces indicated the direction of the stresses were variable within each clevis and between different clevises. It also appears possible that stresses could redistribute and/or change direction as bolt failures progressed at a particular clevis location.

The amount of angled cracking around the bolt OD varied between the bolts from many angled cracks to very minor angled cracking. The amount of angled cracking typically decreases as stresses increases. This suggests that bolts with minor amounts of angled cracking (60°-3, 120°-6, 180°-3, 240°-3, and 300°-1) failed after other bolts at their respective clevis location. Varying amounts of angled cracking could also indicate the presence of a stress concentrator or other surface anomaly, although none were identified in the examined bolts. In all cases, though, fracture was essentially 100% intergranular.

Environment

Alloy X-750 material heat treated using a low temperature solution anneal and two-step aging treatment is known to have poor SCC cracking resistance in both high temperature and low temperature water (Ref. 1). The low temperature crack propagation (LTCP) rates are orders of magnitudes greater than crack growth rates at high temperatures. It should be noted that LTCP will initiate from a crack-like defect, such as a high temperature SCC (HTSCC) defect. LTCP will not initiate from a smooth surface or notch (Ref. 7). This indicates the bolt cracking most likely initiated at high temperatures. Crack propagation may have occurred at high or low temperatures; however, the laboratory testing performed was not unable to conclusively determine the temperature(s) at which crack propagation occurred. In addition, the laboratory data could not determine the age of the cracks, when the cracks initiated, or how fast they propagated.

15.0 CONCLUSIONS

- All of the submitted bolts, including those considered to be intact, contained cracking in the head-to-shank transition. No cracking was identified in the threaded region of any of the bolts.

- There was a generally uniform open crack fracture pattern consisting of crack initiation at two diametrically opposing sides of the bolt in the head-to-shank transition and crack growth that extended upward into the bolt head at a ~35° angle relative to the bolt seating surface. The head separated from the shank when the two opposing cracks linked up near the center of the bolt cross section.

- For each bolt, crack growth occurred along an axis of symmetry created by the opposing directions of crack growth. These crack growth axes indicated the direction of prevailing stresses in each bolt. No correlation between the orientations of the crack growth axes and the in-service orientations of the bolts within each clevis was observed.

- Minor differences in crack morphology around the circumference of the head-to-shank transition suggested that the magnitude of the prevailing stresses varied from bolt to bolt.

- Fractographic SEM analysis and cross section metallographic examinations determined the fracture mode was essentially 100% intergranular with crack branching for all of the bolts.

- The chemical analysis results for all four bolts were consistent with Alloy X-750 material.

- The mechanical properties and microstructure of the bolts were consistent with those published for Alloy X-750 material.

- No unexpected characteristics in the material properties, microstructures, or form of the bolts were identified.

- The laboratory data indicated the bolts failed by intergranular stress corrosion cracking (IGSCC). The reported heat treatment for the bolts included a low solution annealing temperature and two-step aging treatment. Alloy X-750 material heat treated in this manner is known to have poor SCC cracking resistance in both high and low temperature water.

- There was no evidence that the bolts failed due to fatigue cracking or mechanical overload.

16.0 REFERENCES

1. EPRI Materials Handbook, Chapter 2, "Alloy X-750 - Precipitation Hardening Nickel-Base Alloy".

2. ASTM E 8, "Test Methods for Tension Testing of Metallic Materials."

3. ASTM B 637, "Specification for Precipitation-Hardening Nickel Alloy Bars, Forgings, and Forging Stock for High Temperature Service."

4. ASTM A 370, "Test Methods and Definitions for Mechanical Testing of Steel Products."

5. B&W TSG Technical Procedure TP-78, "Tension Testing of Metallic Materials."

6. "Microstructure and Stress Corrosion Resistance of Alloys X-750, 718, and A-286 in LWR Environments, EPRI NP-6392-SD, June 1989.

7. Mills, W.J., et al, "Hydrogen Embrittlement, Grain Boundary Segregation, and Stress Corrosion Cracking of Alloy X-750 in Low- and High-temperature Water", Metallurgical Transactions A, Volume 30A, June 1999.

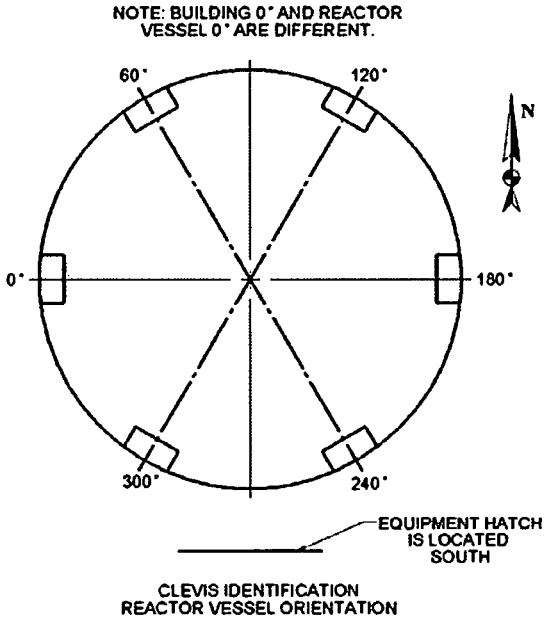

Figure 1: Schematic diagram showing the six clevis locations around the vessel circumference.

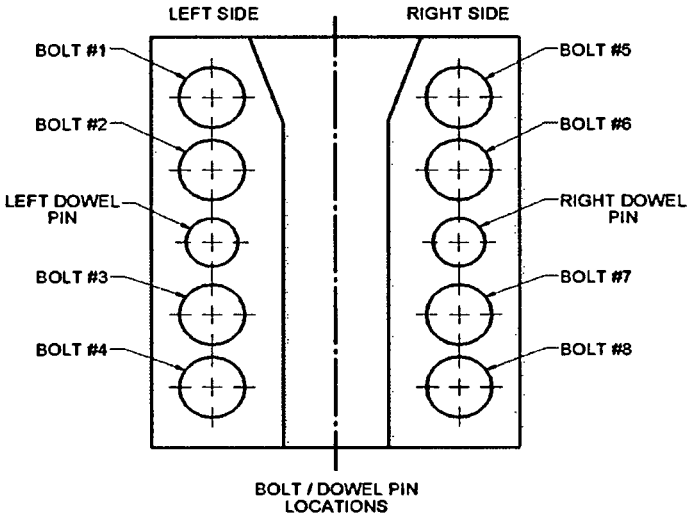

Figure 2: Schematic showing the typical bolt configuration for each clevis insert.

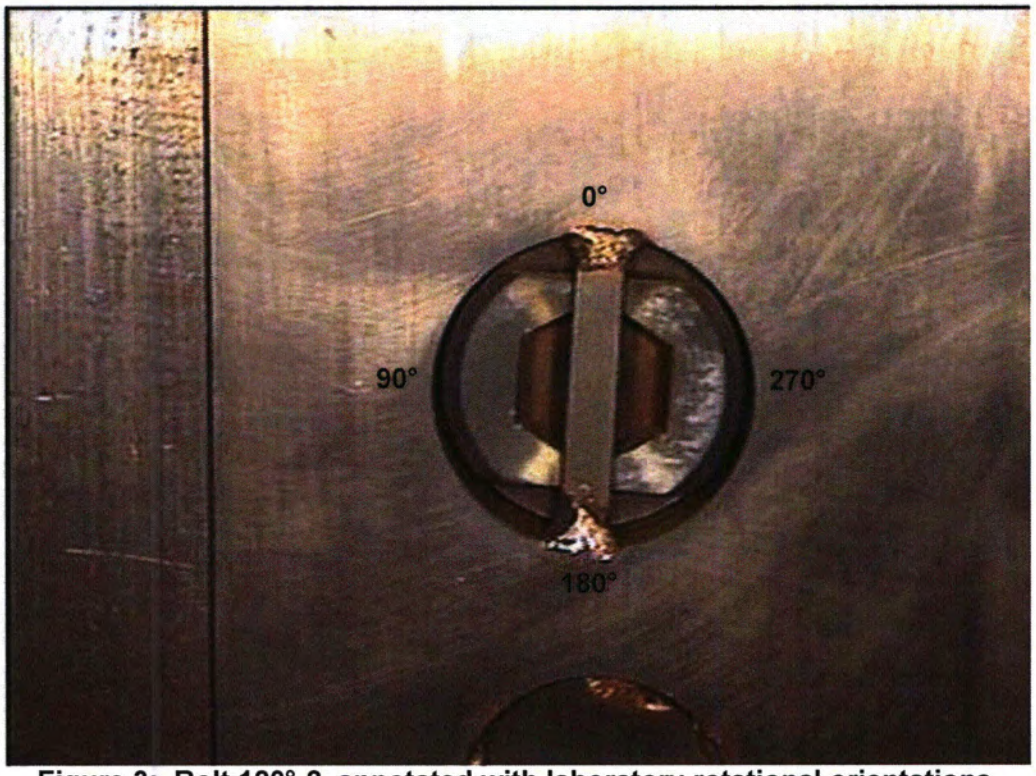

Figure 3: Bolt 120°-2, annotated with laboratory rotational orientations.

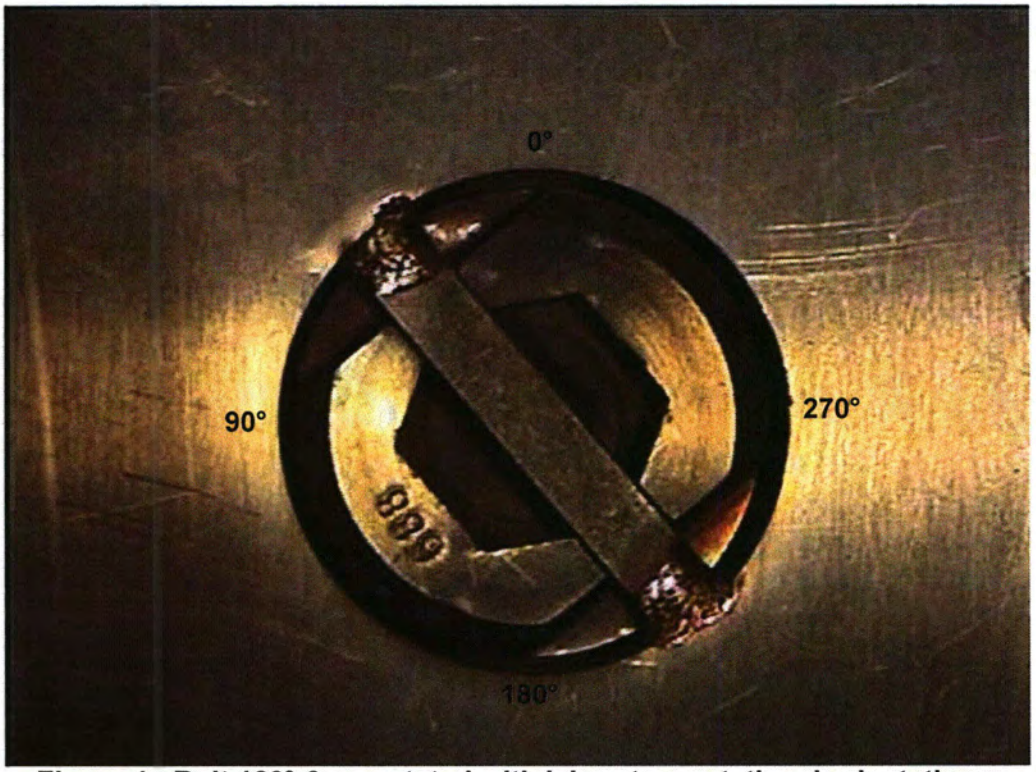

Figure 4: Bolt 120°-6, annotated with laboratory rotational orientations.

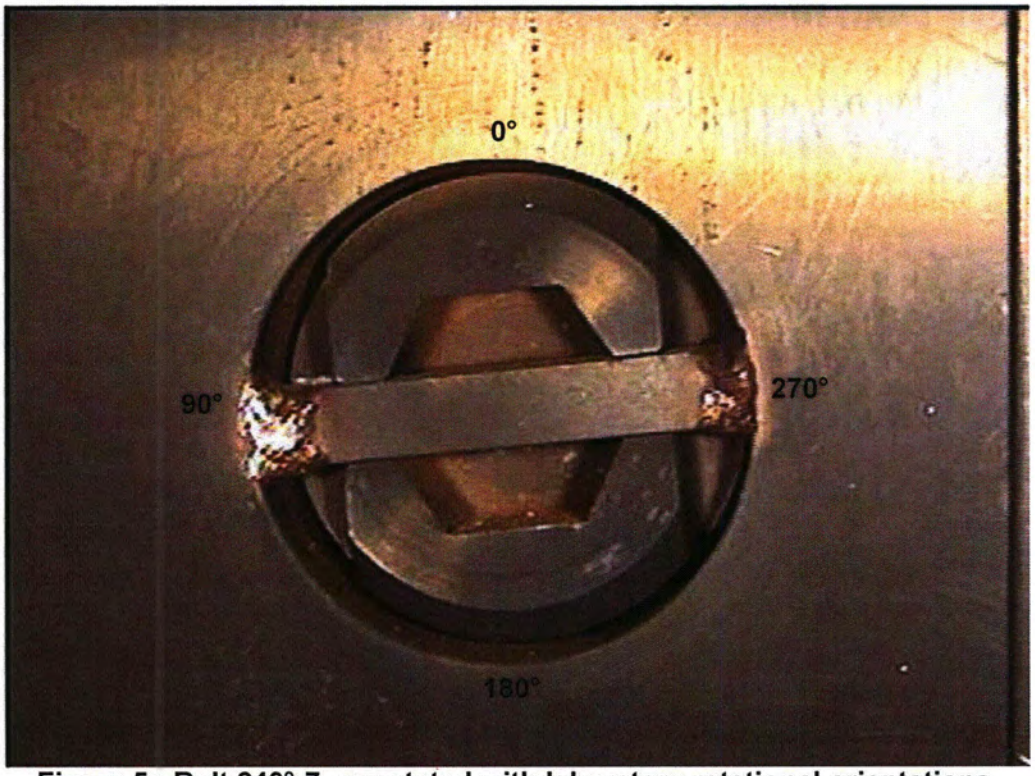

Figure 5: Bolt 240°-7, annotated with laboratory rotational orientations.

Figure 6: Bolt 300°-1, annotated with laboratory rotational orientations.

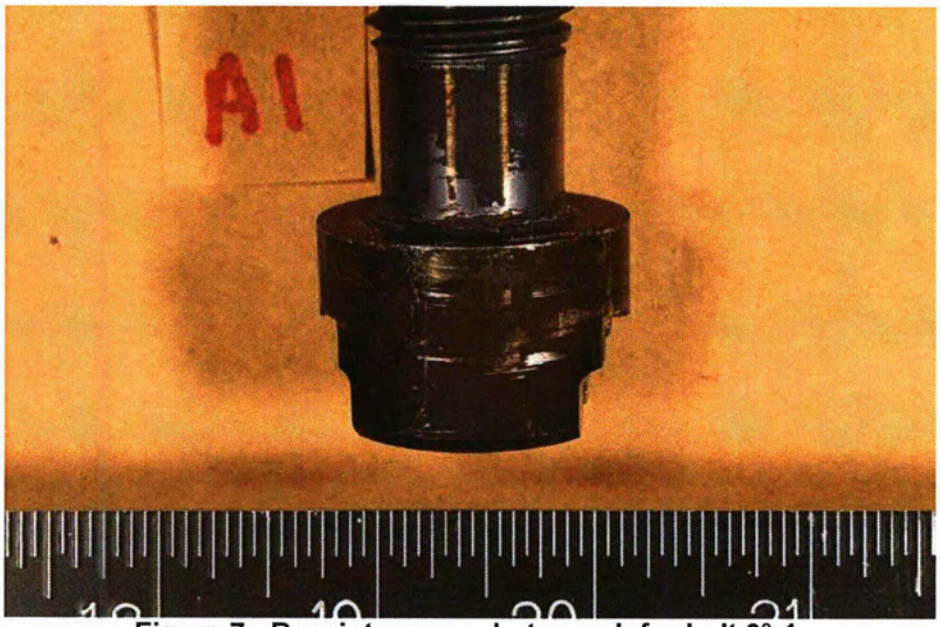

Figure 7: Receipt macro photograph for bolt 0°-1.

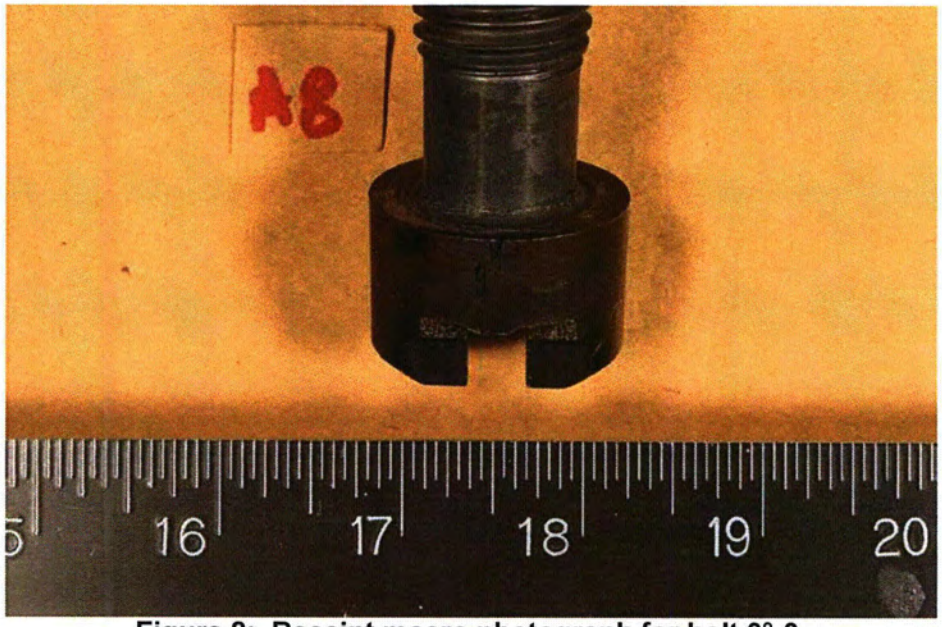

Figure 8: Receipt macro photograph for bolt 0°-3.

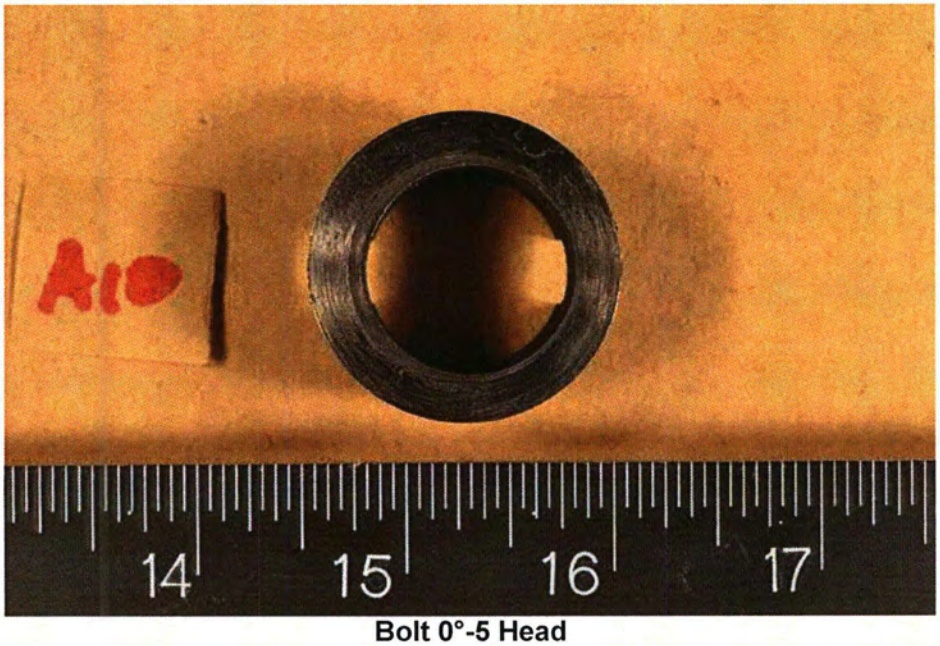

Bolt 0°-5 Head

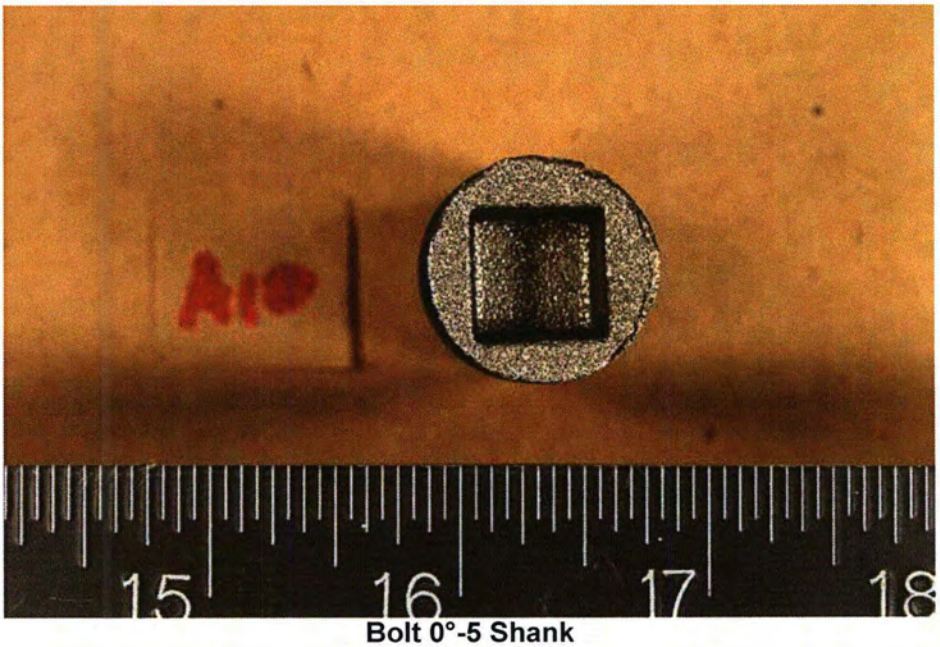

Bolt 0°-5 Shank

Figure 9: Receipt macro photographs for bolt 0°-5.

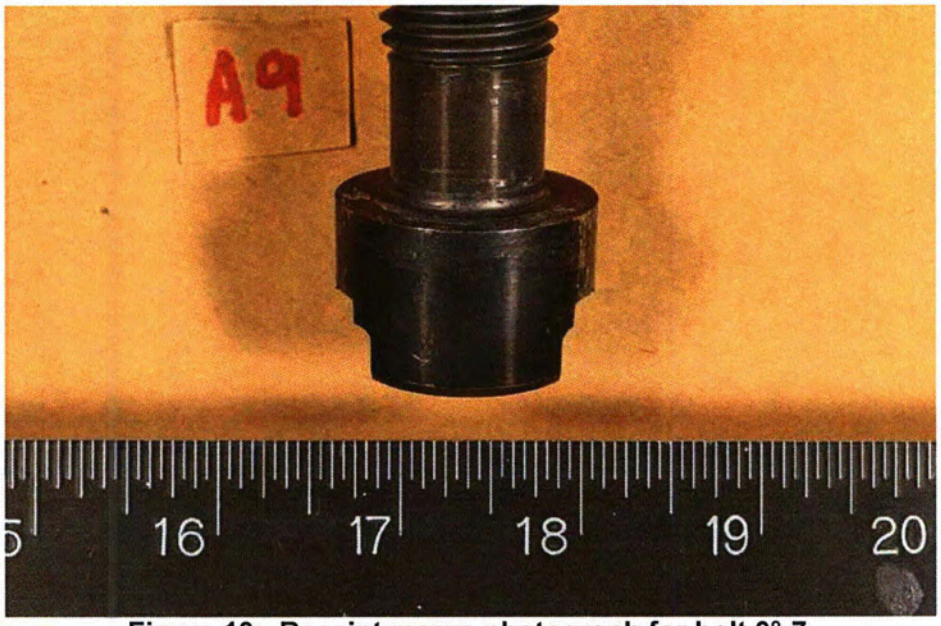

Figure 10: Receipt macro photograph for bolt 0°-7.

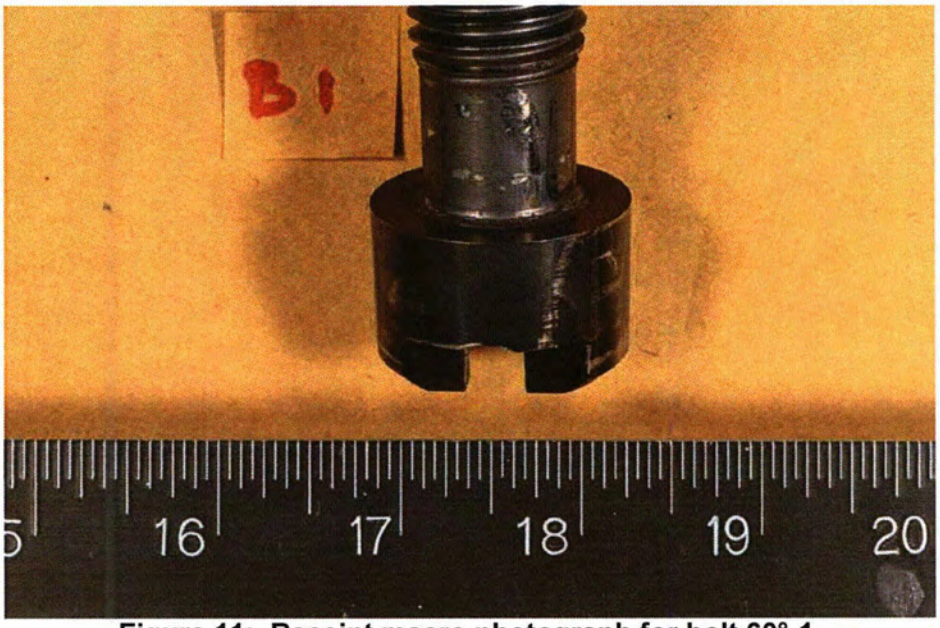

Figure 11: Receipt macro photograph for bolt 60°-1.

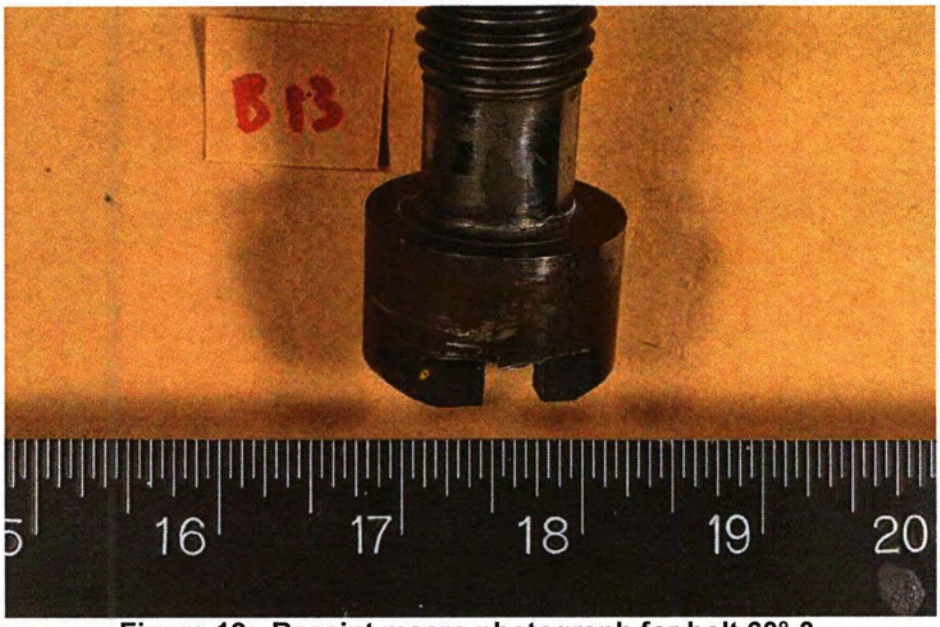

Figure 12: Receipt macro photograph for bolt 60°-3.

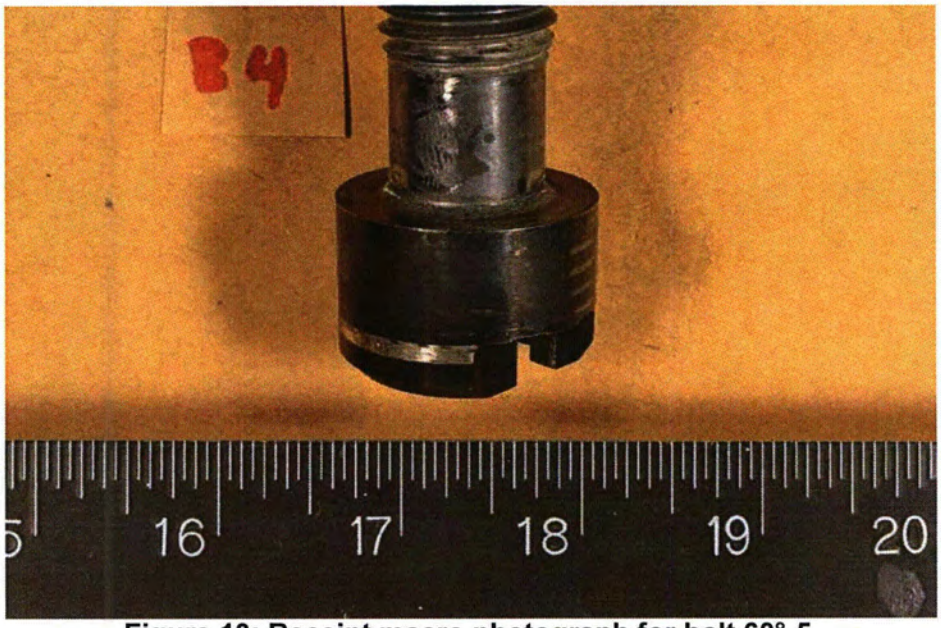

Figure 13: Receipt macro photograph for bolt 60°-5.

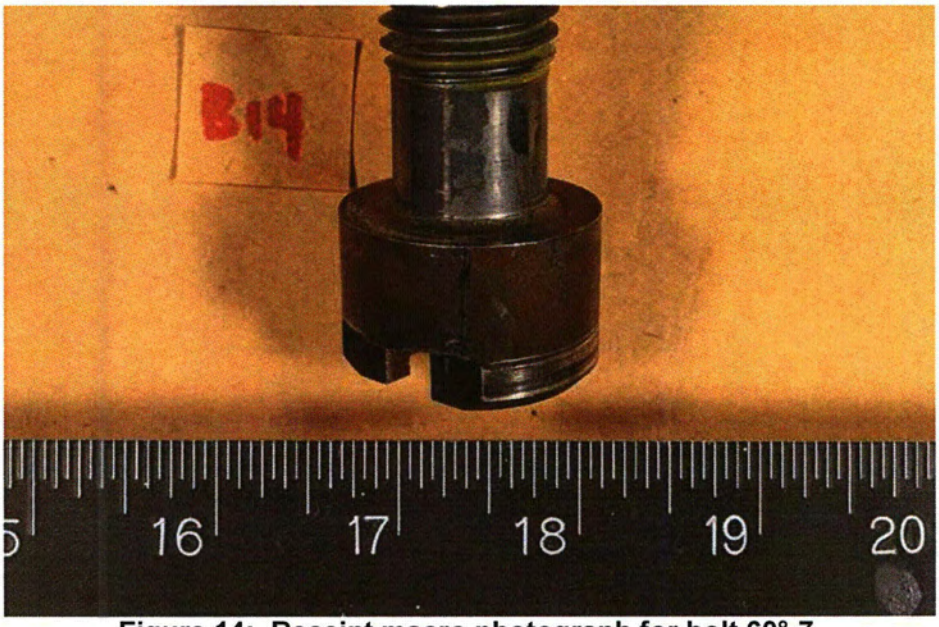

Figure 14: Receipt macro photograph for bolt 60°-7.

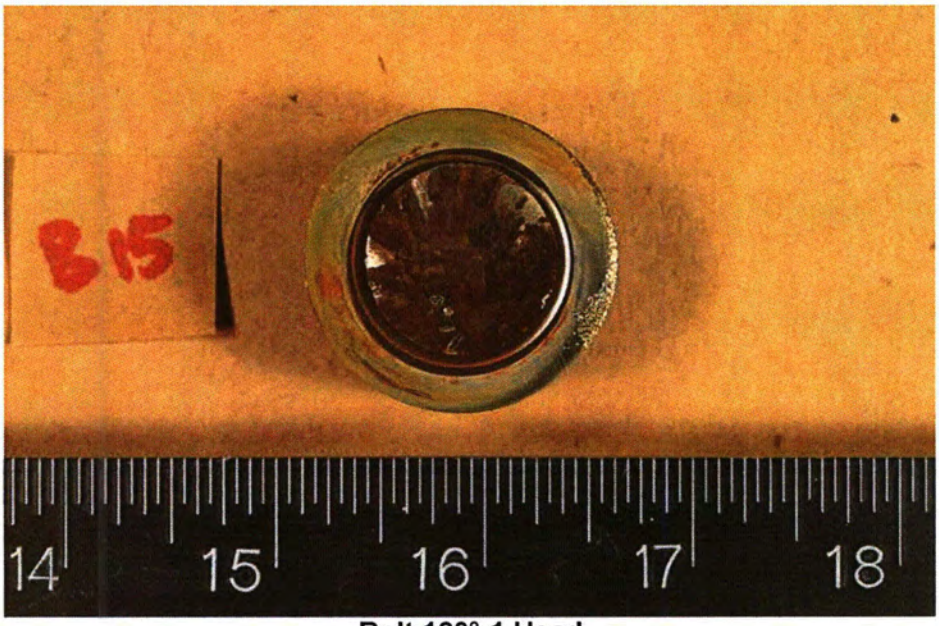

Bolt 120°-1 Head

Bolt 120°-1 Shank

Figure 15: Receipt macro photographs for bolt 120°-1.

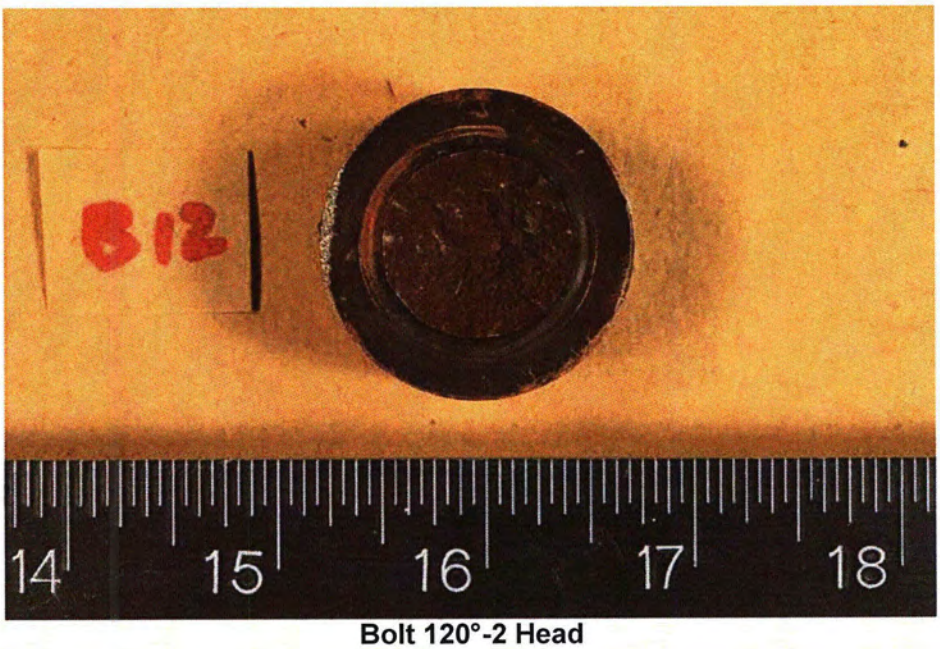

Bolt 120°-2 Head

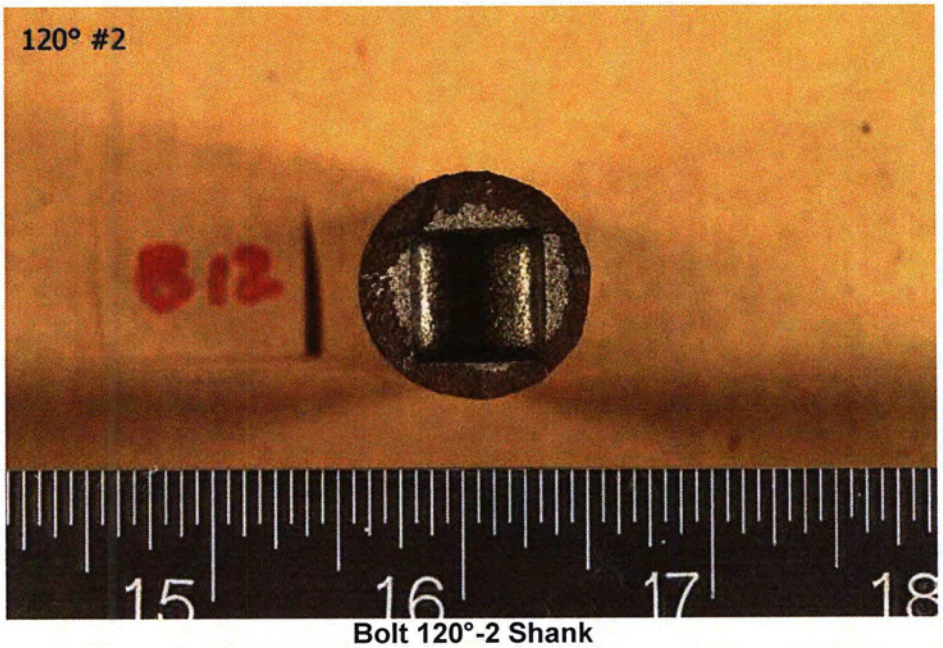

Bolt 120°-2 Shank

Figure 16: Receipt macro photographs for bolt 120°-2.

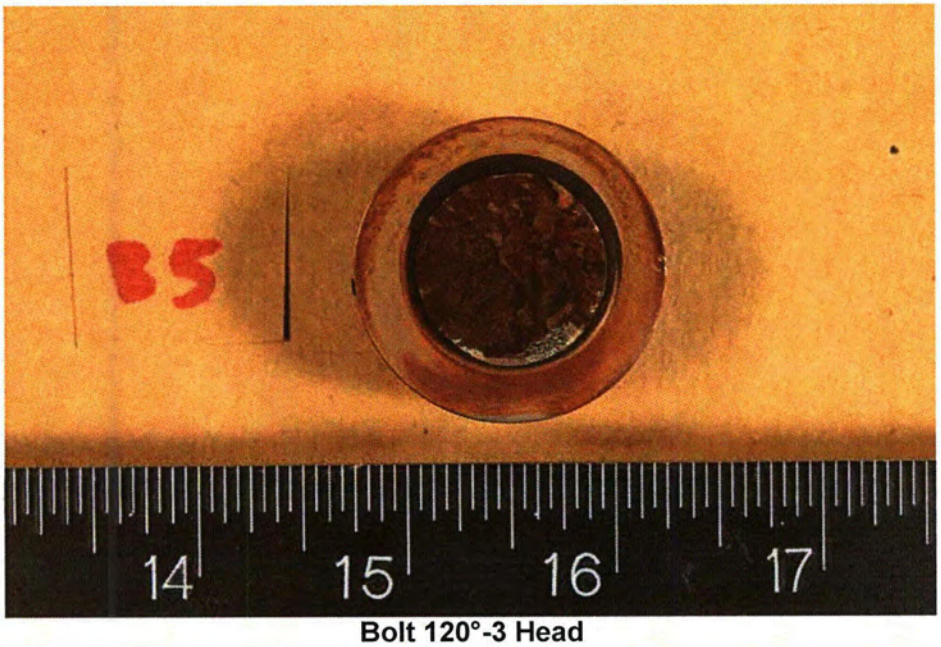

Bolt 120°-3 Head

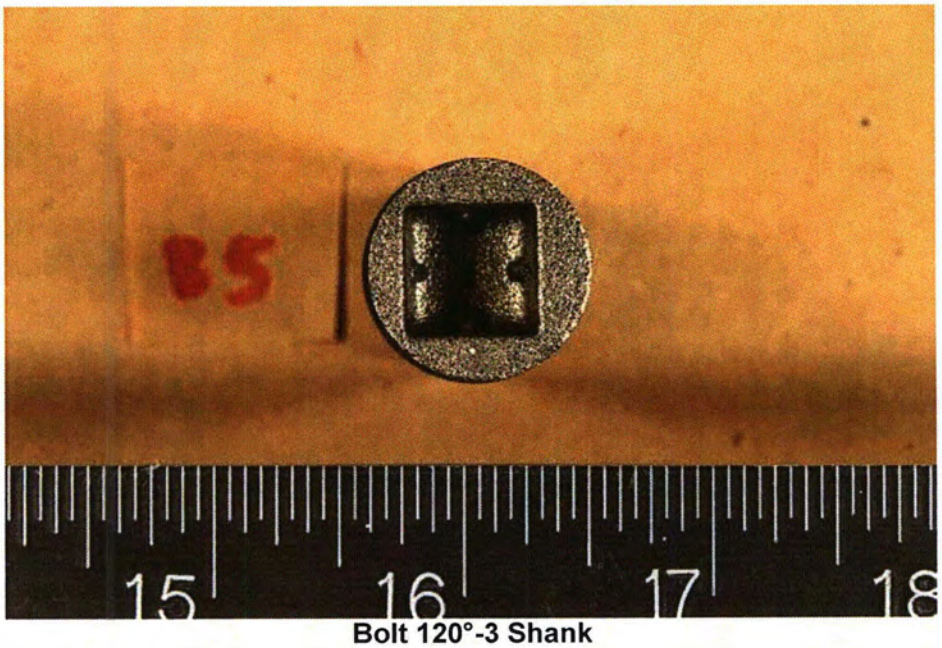

Bolt 120°-3 Shank

Figure 17: Receipt macro photographs for bolt 120°-3.

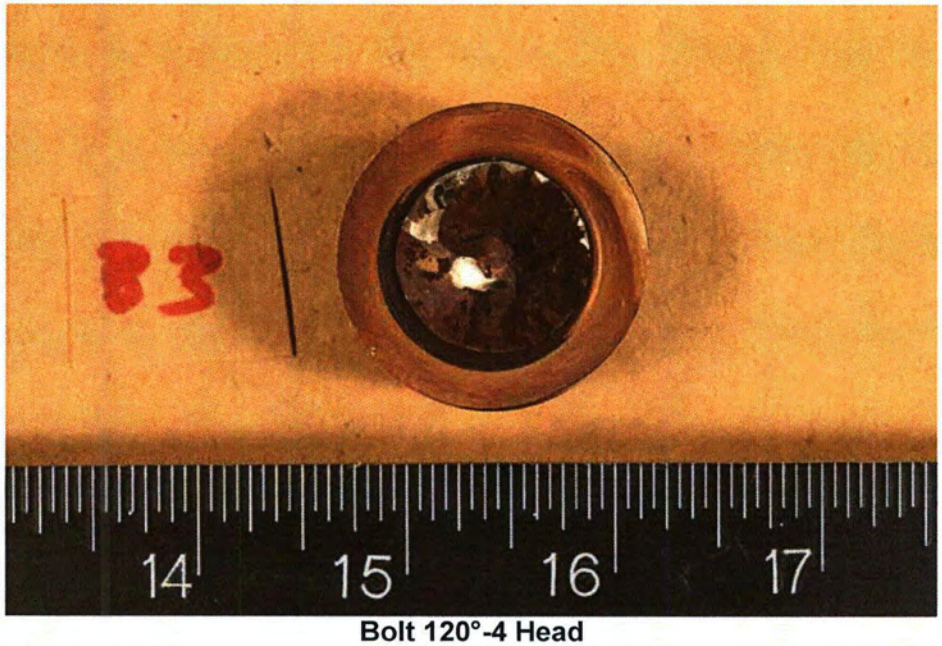

Bolt 120°-4 Head

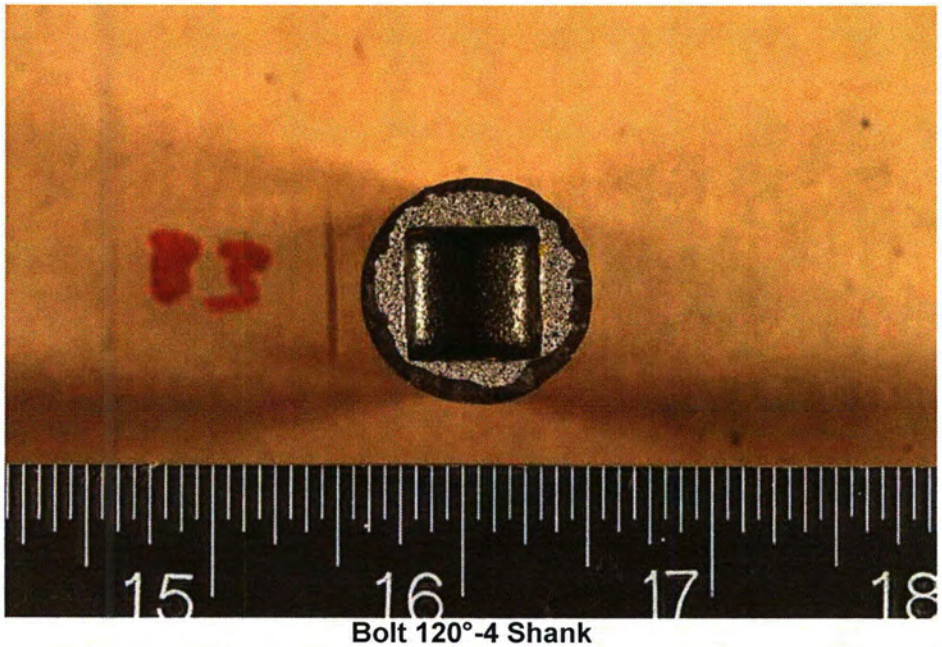

Bolt 120°-4 Shank

Figure 18: Receipt macro photographs for bolt 120°-4.

Bolt 120°-5 Head

Bolt 120°-5 Shank

Figure 19: Receipt macro photographs for bolt 120°-5.

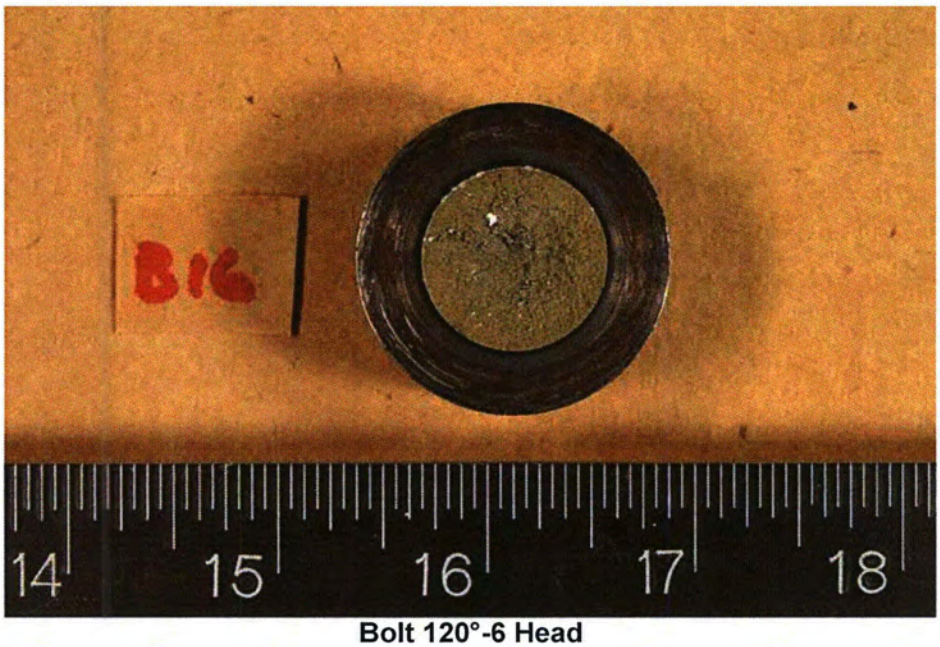

Bolt 120°-6 Head

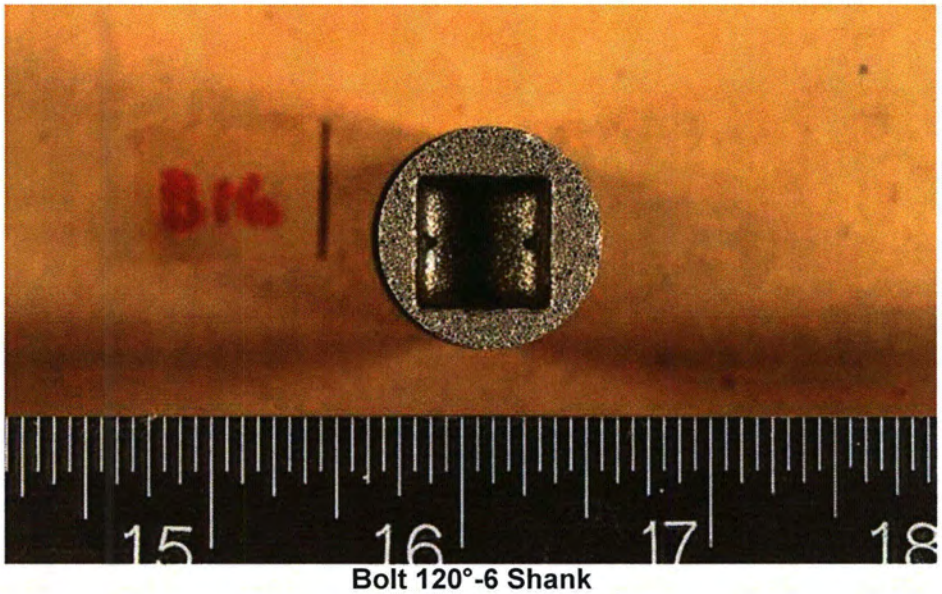

Bolt 120°-6 Shank

Figure 20: Receipt macro photographs for bolt 120°-6.

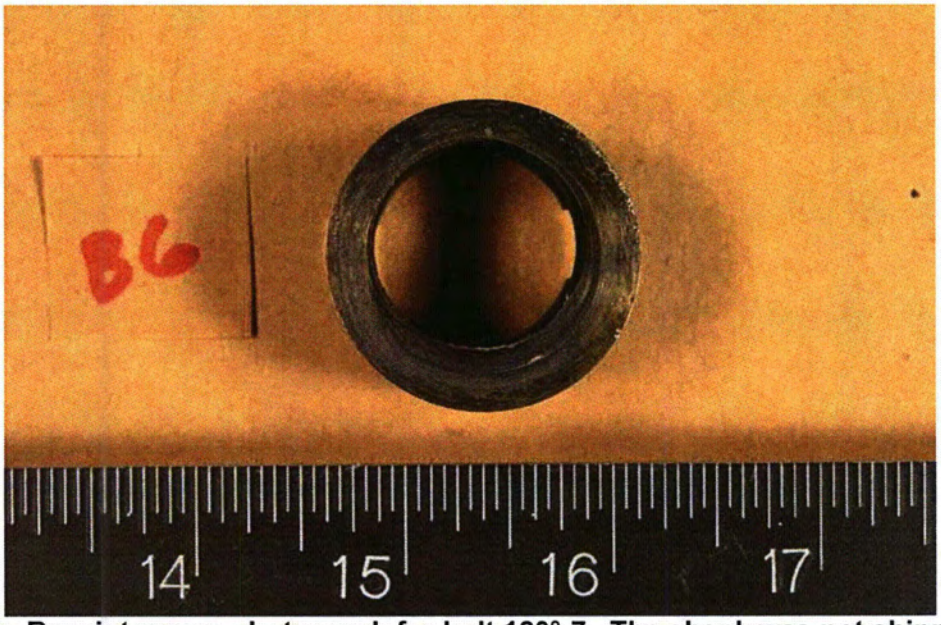

Figure 21: Receipt macro photograph for bolt 120°-7. The shank was not shipped to the laboratory.

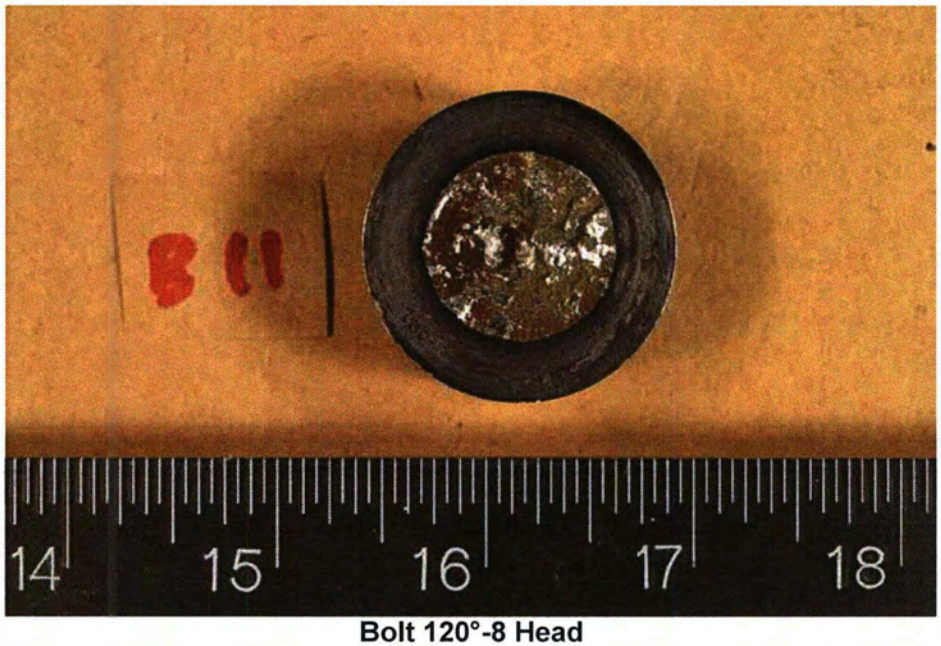

Bolt 120°-8 Head

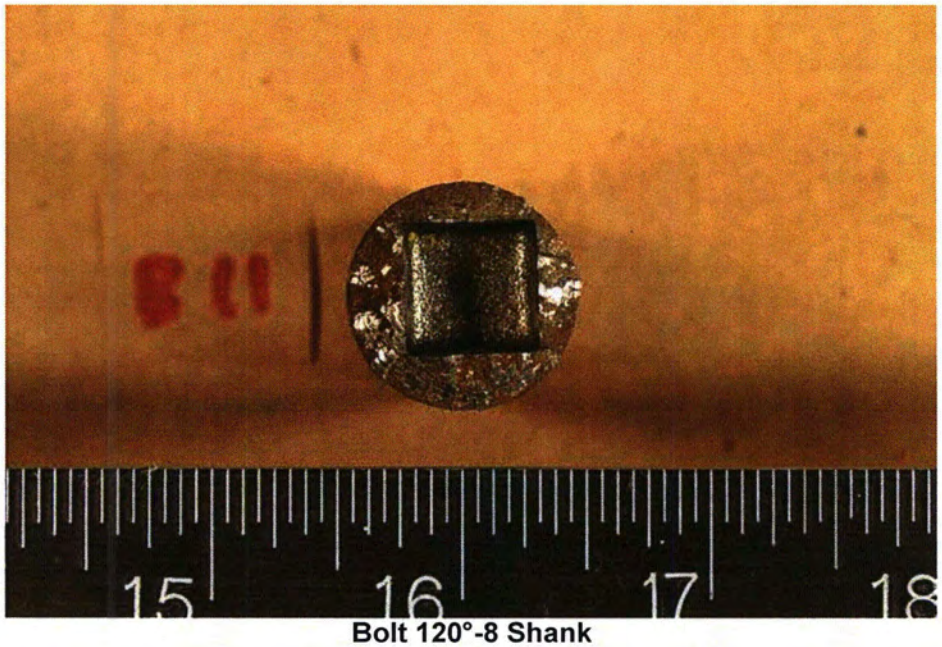

Bolt 120°-8 Shank

Figure 22: Receipt macro photographs for bolt 120°-8.

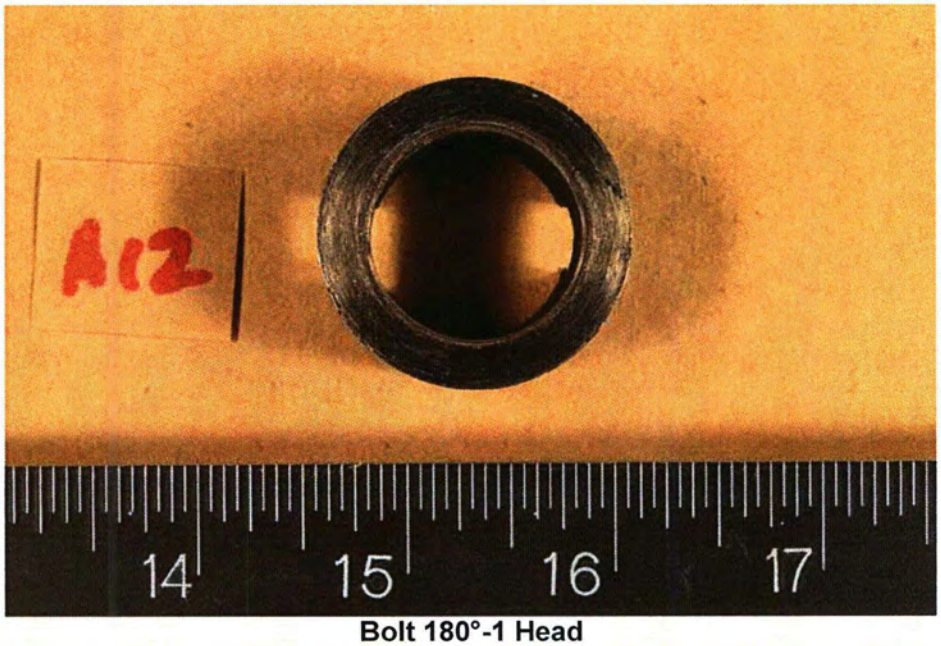

Bolt 180°-1 Head

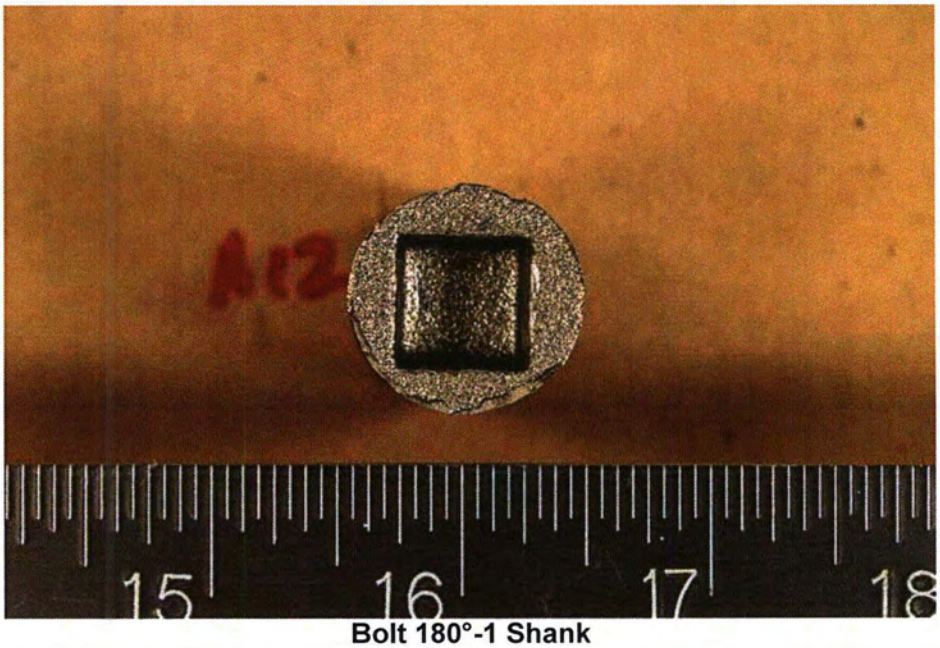

Bolt 180°-1 Shank

Figure 23: Receipt macro photographs for bolt 180°-1.

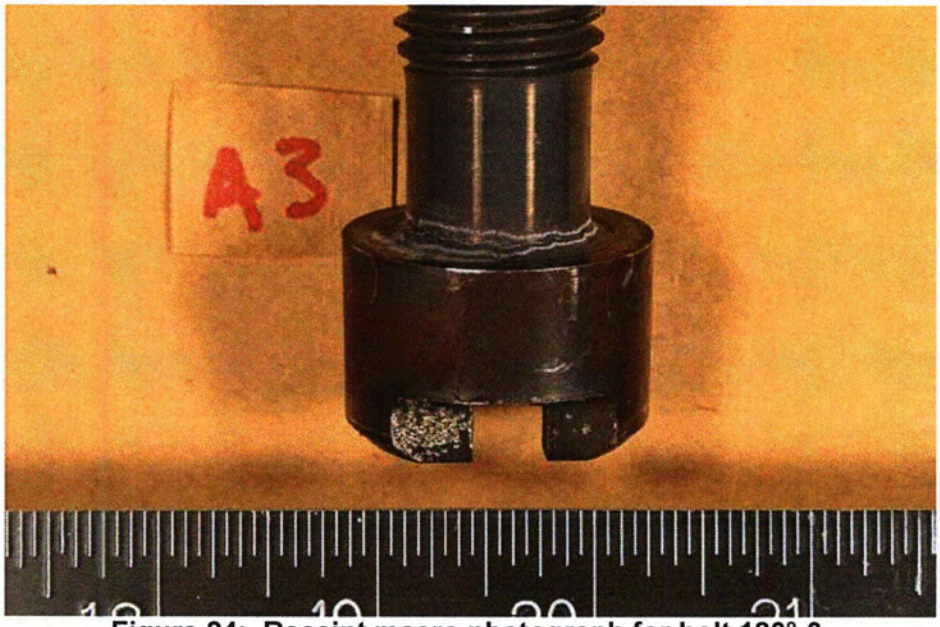

Figure 24: Receipt macro photograph for bolt 180°-3.

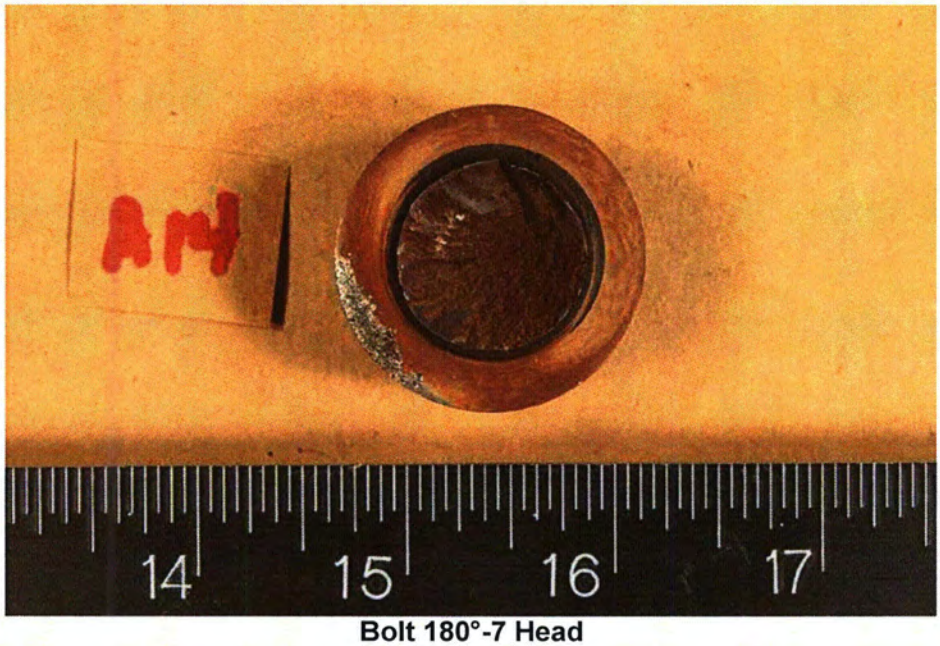

Bolt 180°-7 Head

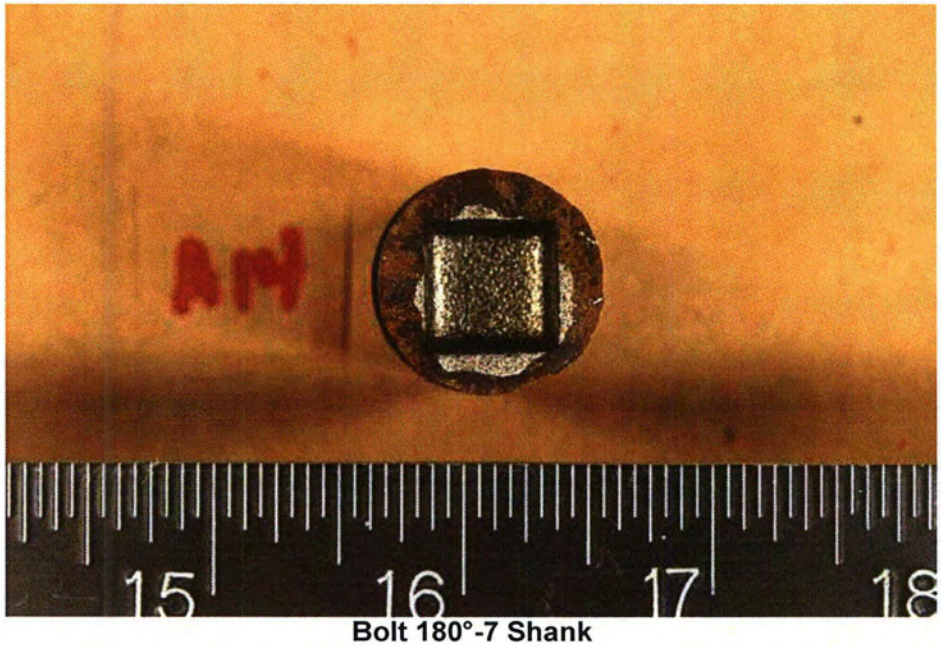

Bolt 180°-7 Shank

Figure 25: Receipt macro photographs for bolt 180°-7.

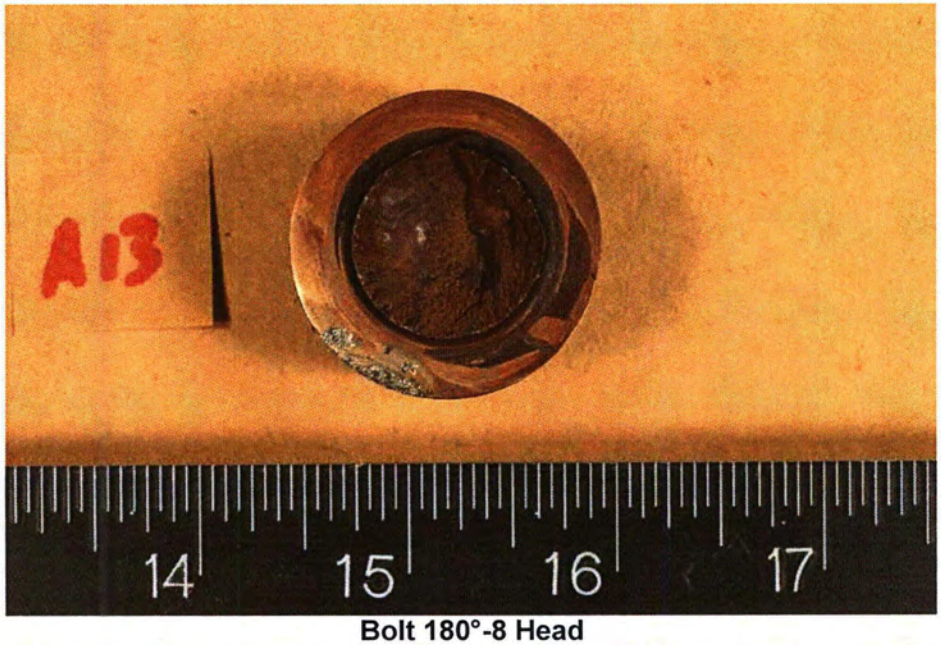

Bolt 180°-8 Head

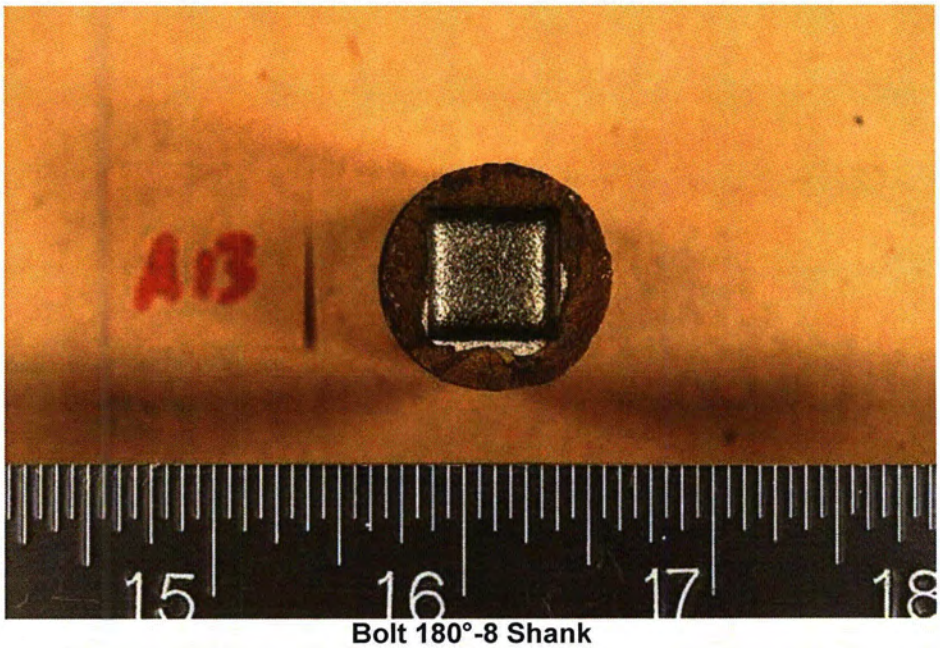

Bolt 180°-8 Shank

Figure 26: Receipt macro photographs for bolt 180°-8.

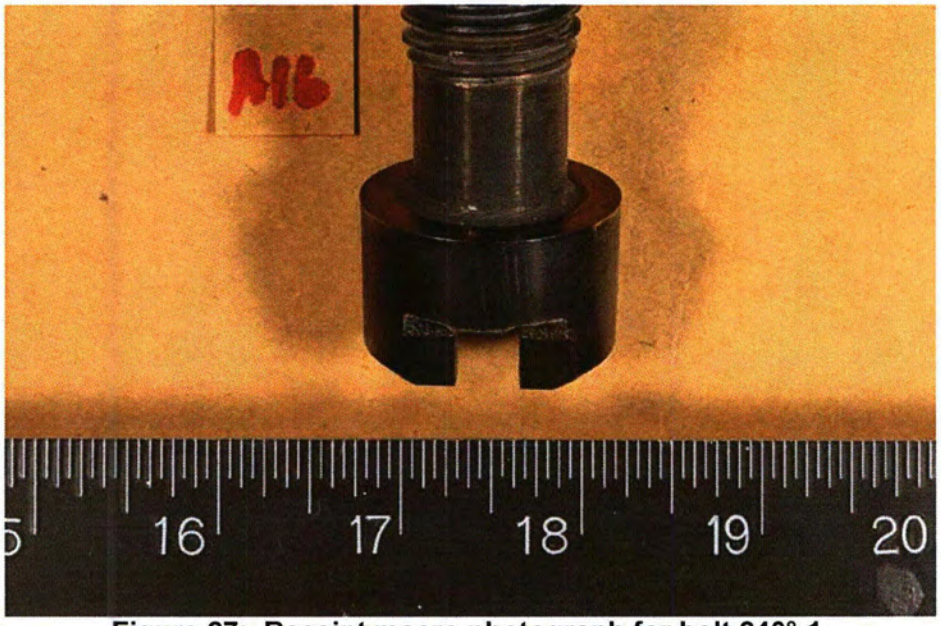

Figure 27: Receipt macro photograph for bolt 240°-1.

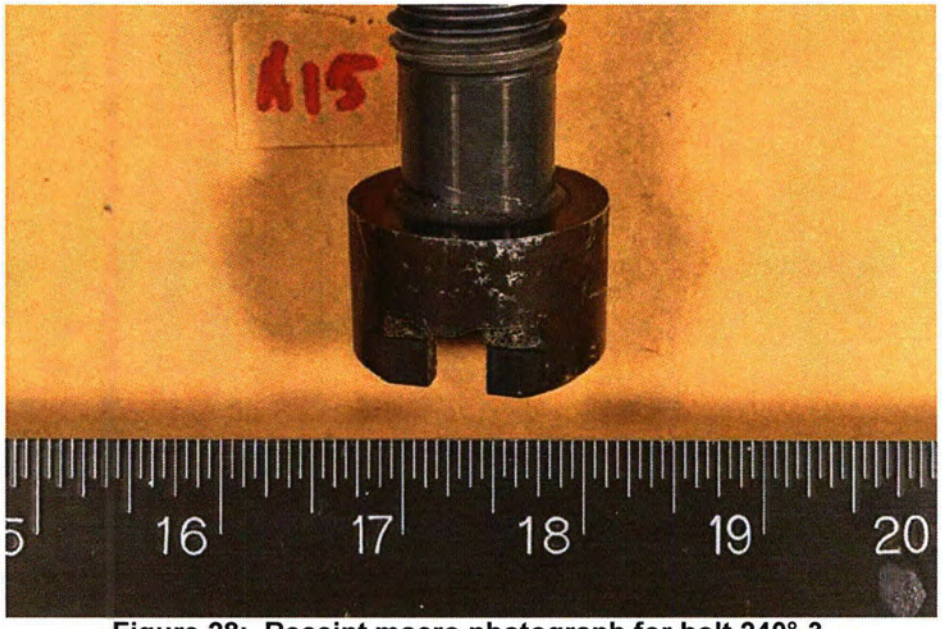

Figure 28: Receipt macro photograph for bolt 240°-3.

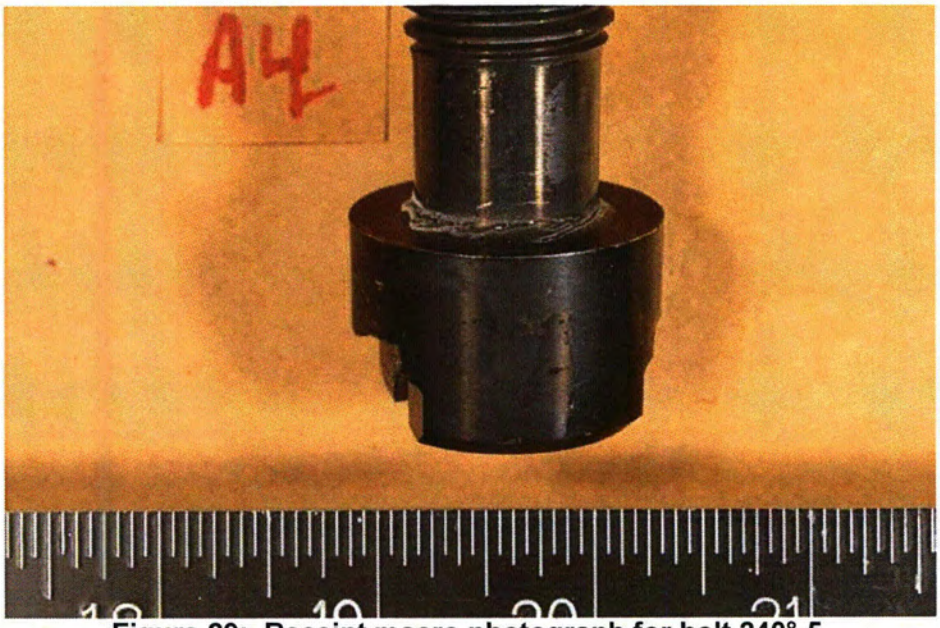

Figure 29: Receipt macro photograph for bolt 240°-5.

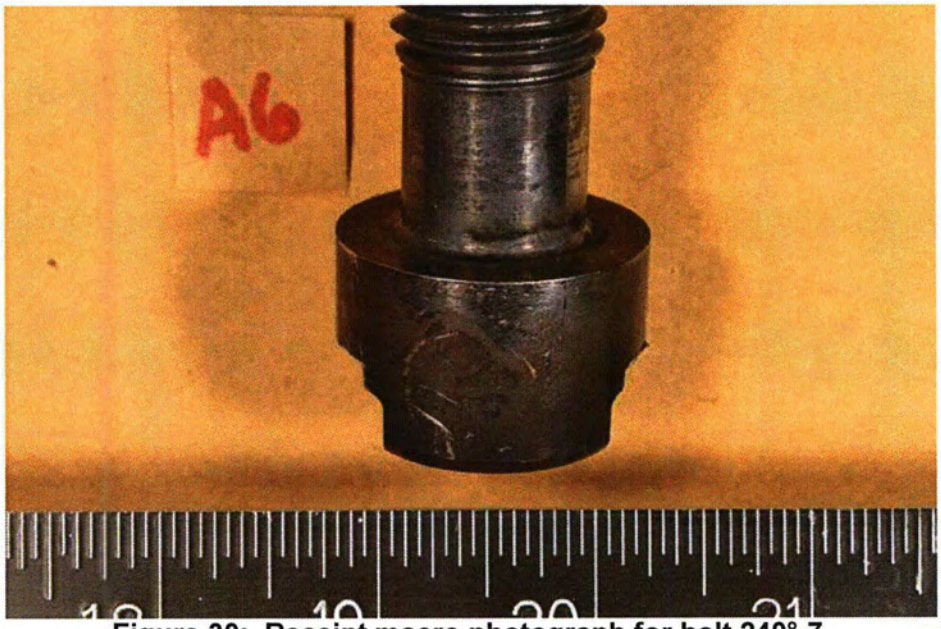

Figure 30: Receipt macro photograph for bolt 240°-7.

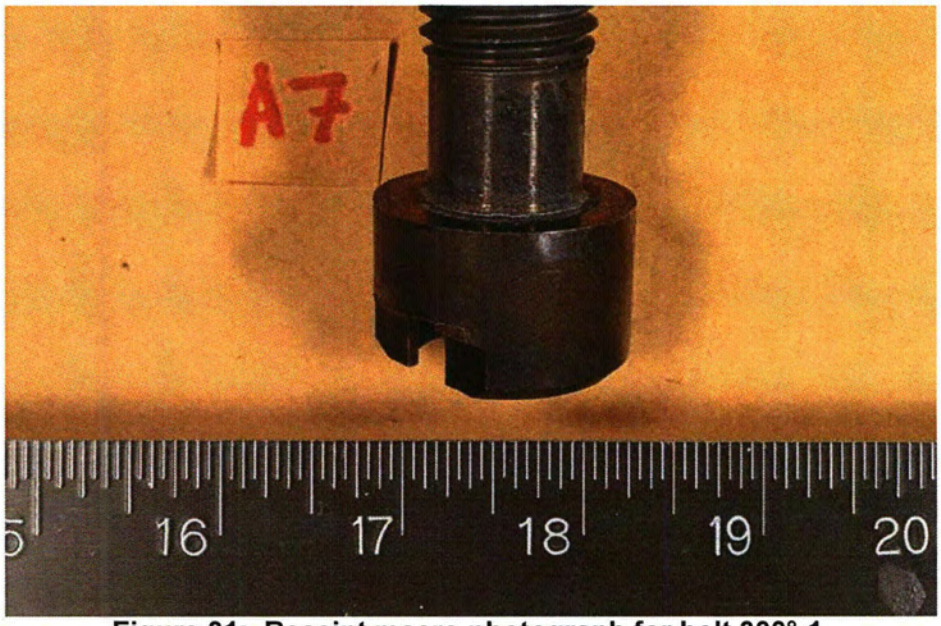

Figure 31: Receipt macro photograph for bolt 300°-1.

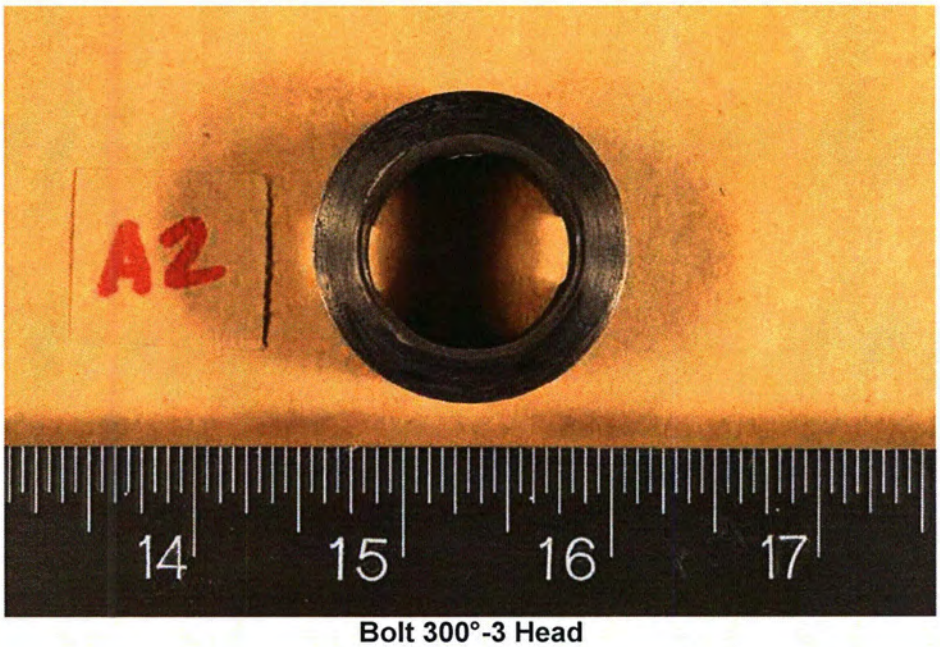

Bolt 300°-3 Head

Bolt 300°-3 Shank

Figure 32: Receipt macro photographs for bolt 300°-3.

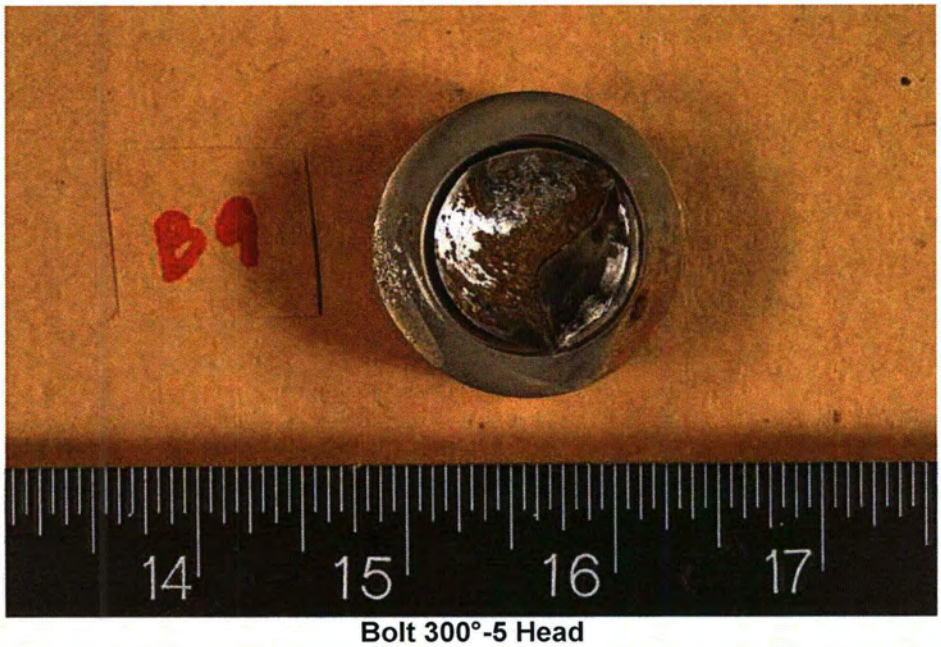

Bolt 300°-5 Head

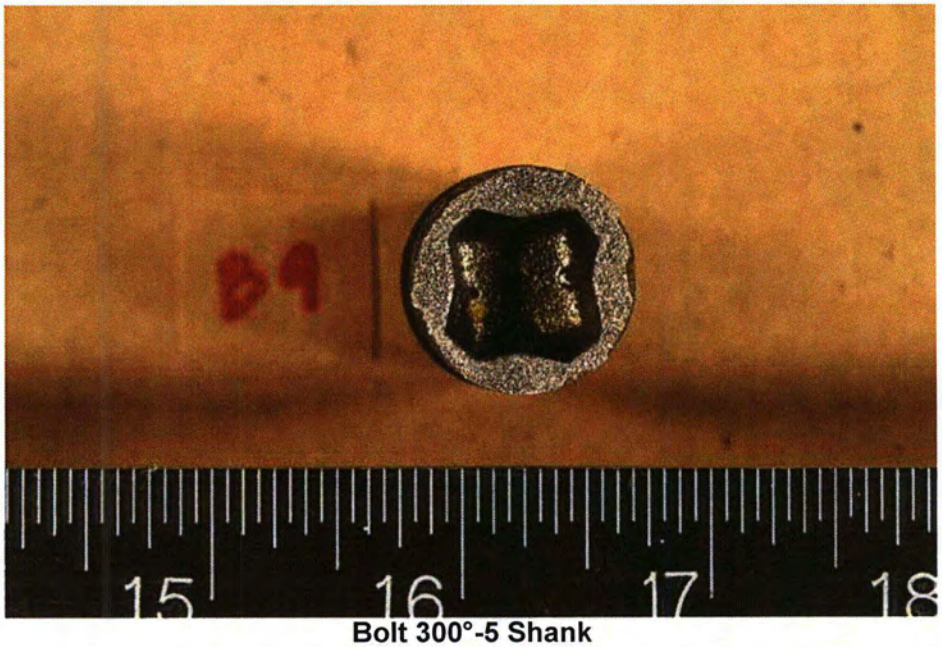

Bolt 300°-5 Shank

Figure 33: Receipt macro photographs for bolt 300°-5.